

Statement for the Use of Animals in Ophthalmic and Vision Research. The ethics committee of our institution approved all surgical interventions and animal care procedures, which were in accordance with the Guidelines and Policies for Animal Surgery provided by the Animal Study Committees of the Central Institute for Experimental Animals of Keio University. Animals received a single intraperitoneal injection of 0.15 mg LPS from *Escherichia coli* (Sigma-Aldrich, St. Louis, MO) in 0.15 mL phosphate-buffered saline (PBS).

### Pretreatment with Telmisartan

Telmisartan was a gift of Boehringer Ingelheim, Ingelheim, Germany. Animals were pretreated with 0.15-mL intraperitoneal injections of vehicle (0.25% dimethylsulfoxide [DMSO] in PBS) or telmisartan daily for 5 days until the injection of LPS. LPS was injected immediately after the fifth telmisartan injection. We dissolved the telmisartan in 30 mM DMSO, diluted to 60  $\mu$ M with PBS and injected into mice at a dose of 10 mg/kg body weight. This dose was sufficient to block AT1-R signaling to decrease systemic blood pressure in rats.<sup>25</sup> The effects of telmisartan pretreatment on ocular inflammation were evaluated 24 hours after LPS injection.

### Lectin Labeling of Retinal Vasculature and Adherent Leukocytes

The retina-adherent leukocytes were imaged by perfusion labeling with fluorescein-*isothiocyanate* (FITC)-coupled concanavalin A lectin (con A; Vector, Burlingame, CA), as described previously.<sup>26</sup> In mice under deep anesthesia, the chest cavity was opened and a 27-gauge cannula was introduced into the left ventricle. After injection of 2 mL of PBS to remove erythrocytes and nonadherent leukocytes, 2 mL FITC-conjugated con A lectin was perfused. After the eyes were enucleated, the retinas were flatmounted. The flatmounts were imaged with an epifluorescence microscope (IX71; Olympus, Tokyo, Japan), and the total number of con A-stained adherent leukocytes per retina was determined.

### Immunohistochemistry for AT1-R

Immunohistochemical experiments were performed with the murine eyes. For histopathologic evaluation, the specimen was fixed with 4% paraformaldehyde (PFA) at 4°C immediately after removal and embedded in paraffin. Three-micrometer paraffin sections were incubated overnight at 4°C with a rabbit polyclonal antibody against human AT1-R (Santa Cruz Biotechnology, Santa Cruz, CA) at a 1:100 dilution. After incubation, they were reacted for 30 minutes at room temperature with goat antibodies against rabbit immunoglobulins (IgGs) conjugated to a peroxidase-labeled dextran polymer (En Vision+ rabbit; Dako Corp., Carpinteria, CA). As a negative control for staining, the first antibodies were replaced with nonimmune rabbit IgGs (Dako). Color was developed with DAB (3,3'-diaminobenzidine tetrahydrochloride; 0.2 mg/mL; Dojindo Laboratories, Kumamoto, Japan) in 0.05 M Tris-HCl (pH 7.6) containing 0.003% hydrogen peroxide, and the sections were counterstained with hematoxylin.

### Aqueous Humor Analyses

Aqueous humor was collected by anterior chamber puncture with a 30-gauge needle at 0, 6, 12, 24, and 48 hours after LPS injection in vehicle- and telmisartan-treated EIU mice. Protein concentration was determined with a protein quantification kit (Dojindo Laboratories), and absorbance was measured with a microplate reader (Bio-Rad Laboratories, Hercules, CA). For evaluation of inflammatory cells in the anterior chamber, 1  $\mu$ L of aqueous-humor samples were dropped on a poly-L-lysine-coated slide (Sigma-Aldrich) and air dried. Slides were processed with Wright's stain, and the total number of cells in each drop was counted under a light microscope, as described previously.<sup>27</sup>

### RT-PCR Analyses

Total RNA was isolated from the retina and the iris-ciliary body complex with extraction reagent (TRIzol; Invitrogen, Carlsbad, CA)

and reverse-transcribed with a cDNA synthesis kit (First-Strand; Amersham Biosciences, Inc., Piscataway, NJ) according to the manufacturer's protocols. PCR was performed with *Taq* DNA polymerase (Toyobo, Tokyo, Japan) in a thermal controller (MiniCycler; MJ Research, Watertown, MA). The primer sequences were as follows: 5'-ATG TGG CAC CAC ACC TTC TAC AAT GAG CTG CG-3' (sense) and 5'-CGT CAT ACT CCT GCT TGC TGA TCC ACA TCT GC-3' (antisense; 837 bp) for  $\beta$ -actin; 5'-TCA CCT GCA TCA TCA TCT GG-3' (sense) and 5'-AGC TGG TAA GAA TGA TTA GG-3' (antisense; 204 bp) for mouse AT1-R; 5'-GTG TCG AGC TTT GGG ATG GTA-3' (sense) and 5'-CTG GGC TTG GAG ACT CAG TG-3' (antisense; 505 bp) for ICAM-1; 5'-TTC CTC TCT GCA AGA GAC T-3' (sense) and 5'-TGT ATC TCT CTG AAG GAC T-3' (antisense; 430 bp) for IL-6; 5'-AGC CCA CGT CGT AGC AAA CCA CCA A-3' (sense) and 5'-ACA CCC ATT CCA TTC ACA GAG CAA T-3' (antisense; 446 bp) for TNF- $\alpha$ ; 5'-TGC ATG TGG CTG TGG ATG TCA TCA A-3' (sense) and 5'-CAC TAA GAC AGA CCC GTC ATC TCC A-3' (antisense; 449 bp) for COX-2; 5'-TCA CGC TTG GGT CTT GTT CAC T-3' (sense) and 5'-TTG TCT CTG GGT CCT CTG GTC A-3' (antisense; 472 bp) for iNOS; and 5'-ATC CCA ATG AGT AGG CTG GAG AG-3' (sense) and 5'-CAG AAG TGC TTG AGG TGG TTG TG-3' (antisense; 617 bp) for MCP-1.

### Western Blot Analysis for AT1-R

The animals were killed with an overdose of anesthesia, and the eyes were immediately enucleated. The retina and the iris-ciliary body complex were carefully isolated and placed into 200  $\mu$ L of lysis buffer (0.02 M HEPES, 10% glycerol, 10 mM Na<sub>4</sub>P<sub>2</sub>O<sub>7</sub>, 100  $\mu$ M Na<sub>3</sub>VO<sub>4</sub>, 1% Triton, 100 mM NaF, and 4 mM EDTA [pH 8.0]) supplemented with protease inhibitors (2 mg/L aprotinin, 100  $\mu$ M phenylmethylsulfonyl fluoride, 10  $\mu$ M leupeptin, and 2.5  $\mu$ M pepstatin A) and sonicated. The lysate was centrifuged at 15,000 rpm for 15 minutes at 4°C, and the supernatants were collected and mixed with sample buffer. Each sample containing 50  $\mu$ g of total protein was then boiled for 5 minutes, separated by sodium dodecyl sulfate-polyacrylamide gel electrophoresis SDS-PAGE, and electroblotted to polyvinylidene fluoride (PVDF) membrane (Millipore Corp., Bedford, MA). After nonspecific binding was blocked with 5% bovine serum albumin, the membranes were incubated with a rabbit anti-human AT1-R polyclonal antibody (1:100; Santa Cruz Biotechnology) at room temperature for 1 hour, followed by incubation with a horseradish-peroxidase-conjugated goat antibody directed against rabbit IgGs (1:5000; BioSource, Camarillo, CA). The signals were visualized with an enhanced chemiluminescence kit (ECL; Amersham Biosciences, Inc.) according to the manufacturer's protocol.

### Enzyme-Linked Immunosorbent Assay for ICAM-1

The animals were killed with an overdose of anesthesia, and the eyes were immediately enucleated. The retina was carefully isolated and placed into 200  $\mu$ L of lysis buffer supplemented with protease inhibitors and sonicated. The lysate was centrifuged at 15,000 rpm for 15 minutes at 4°C, and the ICAM-1 level in the supernatant was determined with the mouse ICAM-1 kit (R&D Systems Inc., Minneapolis, MN) according to the manufacturer's protocol. The tissue sample concentration was calculated from a standard curve and corrected for protein concentration.

### Morphometric and Statistical Analyses

All results are expressed as the mean  $\pm$  SD. The number of leukocytes in each flatmount was counted independently by two investigators with the epifluorescence microscope. The data were processed for statistical analyses (Mann-Whitney test). Differences were considered to be statistically significant at  $P < 0.05$ .

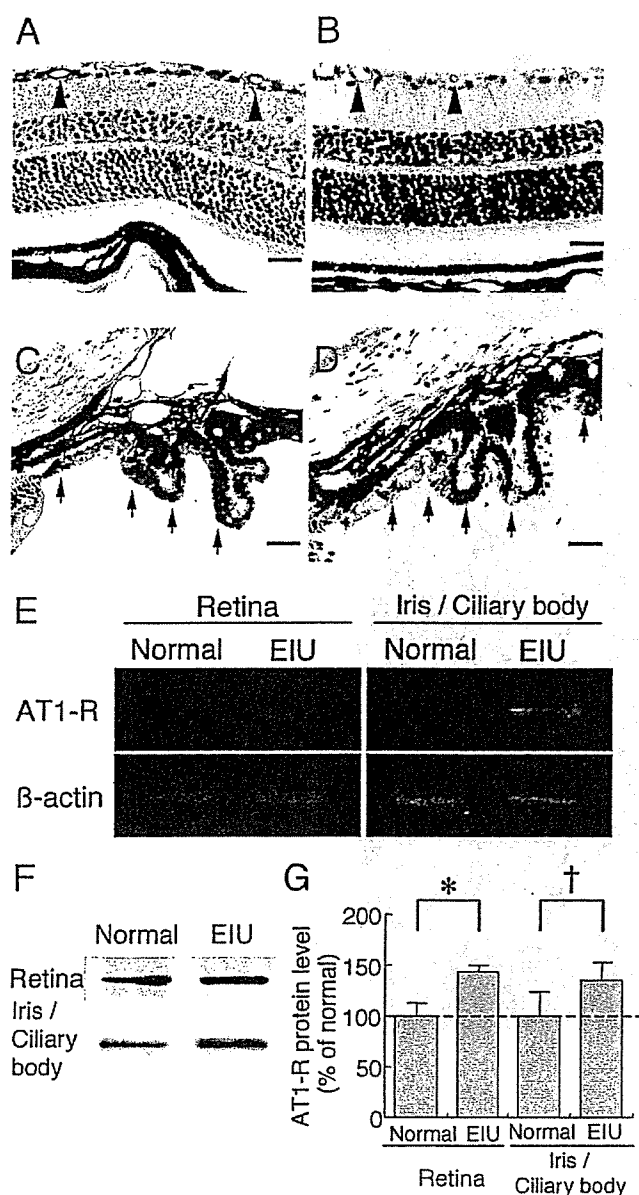


**FIGURE 1.** AT1-R tissue localization and induction in EIU. Immunohistochemical staining (A–D), RT-PCR (E), and Western blot analysis (F, G) of AT1-R expression in the retina and the iris-ciliary body complex. Retinal sections from normal (A) and EIU (B) mice. Positive staining for AT1-R on the inner retinal vessels (A, B, arrows). Sections of iris-ciliary body complex from normal (C) and EIU (D) mice. Positive staining for AT1-R on the nonpigmented epithelial cells of the ciliary body (C, D, arrows). Scale bar, 100  $\mu$ m. AT1-R mRNA (E) and protein (F, G) levels of the retina and iris-ciliary body in EIU mice were higher than those in normal age-matched mice. The results represent the mean  $\pm$  SD;  $n = 6$ . \* $P < 0.01$ , † $P < 0.05$ , by Mann-Whitney test.

**RESULTS**

**AT1-R Tissue Localization and Upregulation in EIU**

Immunohistochemistry for AT1-R was performed to identify its expression in the eyes in normal (Figs. 1A, 1C) and EIU (Figs. 1B, 1D) mice. AT1-R immunoreactivity was detected mainly on the endothelial cells of inner retinal vessels (Figs. 1A, 1B) and nonpigmented epithelial cells of the ciliary body (Figs. 1C, 1D). Retinas and iris-ciliary body complex were subjected to RT-

PCR and Western blot analyses to detect the expression of AT1-R at mRNA (Fig. 1E) and protein (Figs. 1F, 1G) levels, respectively. AT1-R mRNA and protein levels of the retina and the iris-ciliary body complex in EIU mice were significantly higher than in normal, age-matched animals.

**Effects of Telmisartan on Retinal Leukocyte Adhesion**

The retina-adherent leukocytes were imaged by perfusion labeling with FITC-coupled con A. Leukocyte counts were evaluated in the posterior retina around the optic disc (Figs. 2A–D), the midperipheral retina near the equator of the globe (Figs. 2E–H), and the peripheral (anterior) retina next to the ora serrata (Figs. 2I–L). Retina-adherent leukocytes, which were few in normal mice (Figs. 2A, 2E, 2I), increased with induction of EIU (Figs. 2B, 2F, 2J). Compared with vehicle-treated EIU retina (Figs. 2C, 2G, 2K), telmisartan administration (Figs. 2D, 2H, 2L) suppressed leukocyte adhesion in the EIU retina. The total number of adherent leukocytes in nontreated EIU mice ( $125.3 \pm 30.5$ ) was significantly ( $P < 0.01$ ) higher than in normal age-matched control animals ( $4.4 \pm 2.1$ ). Telmisartan-treated EIU mice showed a significant ( $P < 0.01$ ) decrease in leukocyte counts (to  $62.5 \pm 12.0$ ), compared with vehicle-treated EIU mice (to  $116.0 \pm 20.1$ ) or nontreated EIU mice (to  $125.3 \pm 30.5$ ) (Fig. 2M).

**Effects of Telmisartan on Retinal ICAM-1 Expression**

Retinal ICAM-1 expression at mRNA and protein levels was analyzed by RT-PCR (Fig. 3A) and ELISA (Fig. 3B), respectively. Retinal ICAM-1 mRNA expression in nontreated and vehicle-treated EIU mice was higher than in normal age-matched control animals. Systemic administration of telmisartan substantially reduced ICAM-1 mRNA expression (Fig. 3A). Similarly, retinal ICAM-1 protein levels were significantly attenuated after pretreatment with telmisartan ( $P < 0.05$ , Fig. 3B).

**Effects of Telmisartan on Retinal Expression of Inflammatory Mediators**

To determine whether telmisartan affects inflammatory mediators associated with the pathogenesis of EIU, we analyzed retinal mRNA expression of IL-6, TNF- $\alpha$ , COX-2, iNOS, and MCP-1 at 6 hours after LPS injection by RT-PCR (Fig. 4). Retinal mRNA expressions of these agents in vehicle-treated EIU mice were higher than in normal age-matched control mice. Systemic administration of telmisartan substantially reduced expression of their mRNA.

**Effects of Telmisartan on Anterior Chamber Protein Leakage and Leukocyte Infiltration**

Telmisartan pretreatment led to suppression of leukocyte adhesion to the retinal vasculature in the posterior to anterior (peripheral) region, showing its anti-inflammatory effects on the posterior and intermediate segments of the globe. To evaluate its anti-inflammatory effect on anterior uveitis, we analyzed protein leakage and leukocyte infiltration into the aqueous humor. Protein concentration and leukocyte counts in the aqueous humor of the telmisartan-treated EIU mice were compared with that in vehicle-treated EIU mice (Fig. 5). Telmisartan-treated EIU mice showed a significant ( $P < 0.01$ ) decrease in the cell counts at 12 and 24 hours after LPS injection, compared with vehicle-treated EIU mice (Fig. 5A). Protein concentration in the aqueous humor of the telmisartan-treated EIU mice at 12 and 24 hours after LPS injection tended to be lower than that of vehicle-treated EIU mice, but the difference was not statistically significant (Fig. 5B).

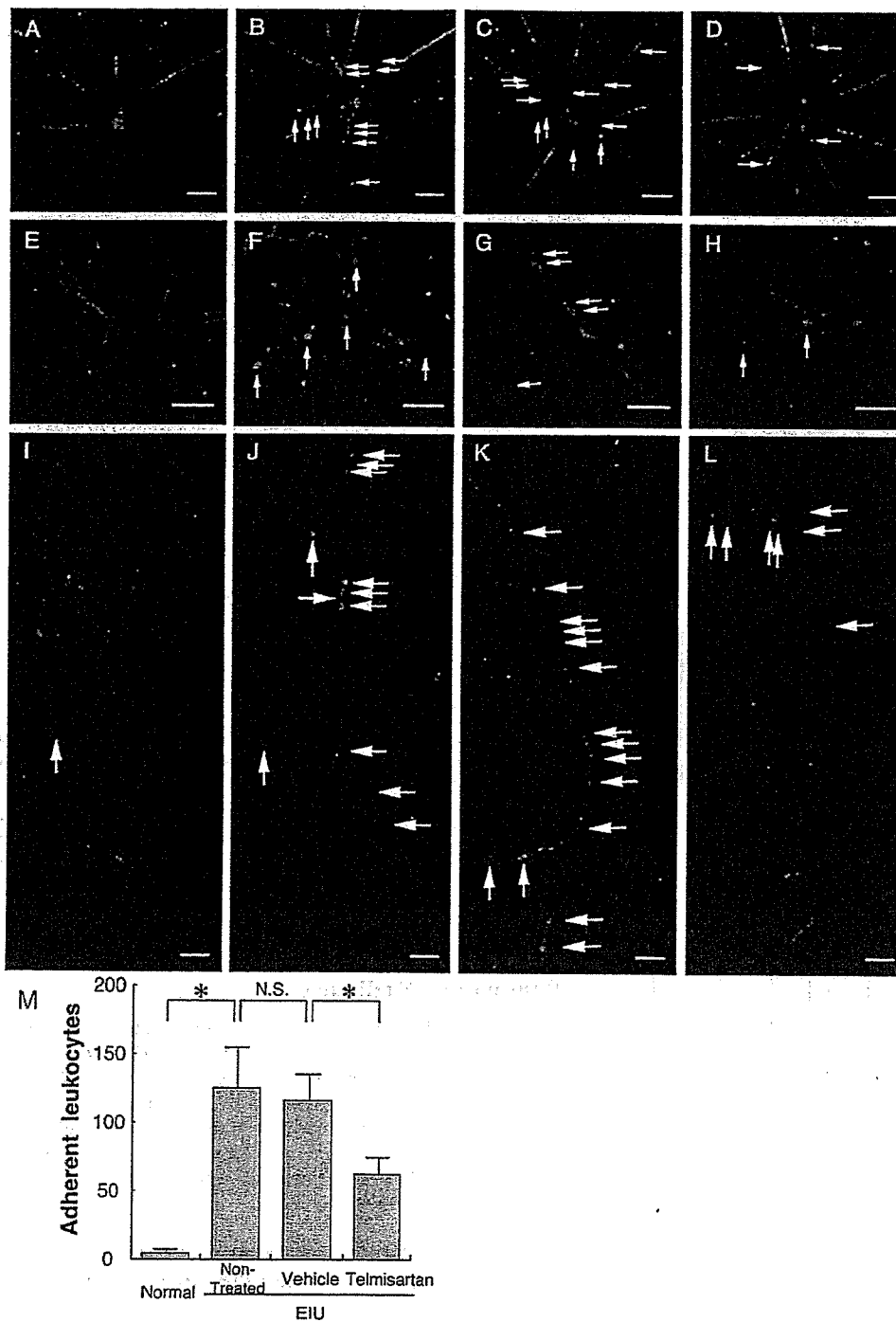


**FIGURE 2.** Effects of telmisartan on retinal inflammation. Flatmounted retinas from normal mice (A, E, I), nontreated EIU mice (B, F, J), vehicle-treated EIU mice (C, G, K), and telmisartan-treated EIU mice (D, H, L). Nontreated and vehicle-treated EIU mice showing increased adherent leukocytes (arrows) compared with normal mice. The treatment with telmisartan decreased the adherent leukocytes. Scale bar, 100  $\mu\text{m}$ . (M) Quantification of adherent retinal leukocytes. Telmisartan-treated EIU mice showed significantly fewer adherent leukocytes than did nontreated or vehicle-treated mice. The results represent the mean  $\pm$  SD;  $n = 15$ . \* $P < 0.01$  by Mann-Whitney test.

## DISCUSSION

The present study demonstrates for the first time that AT1-R upregulation is associated with ocular inflammation in the murine model of EIU and that the AT1-R signaling blockade with telmisartan attenuates several inflammatory parameters including ICAM-1-mediated leukocyte adhesion and infiltration in EIU eyes.

Leukocyte adhesion to the vessel walls is an important process in inflammation. When leukocytes are recruited to inflammatory sites, adhesion molecules play essential roles in the first phase of inflammation. ICAM-1 and its counter receptor  $\beta 2$  (CD18)-integrins (i.e., LFA-1 and Mac-1) regulate the leukocyte-endothelial interaction in the pathogenesis of

EIU.<sup>8-10</sup> During the development of EIU, ICAM-1 is upregulated and expressed on vascular endothelial cells of the iris-ciliary body shortly after LPS injection.<sup>9</sup> In addition, several studies have demonstrated that treatment with anti-ICAM-1 antibodies significantly inhibits the development of EIU.<sup>9,10</sup> In the present study, upregulation of retinal ICAM-1 in EIU was suppressed after pretreatment with telmisartan. This finding is supported by recent data from in vitro assays and in vivo models on systemic hypertension and diabetes, showing that AT1-R blockade attenuates ICAM-1 expression.<sup>19,28</sup> Recently, we have demonstrated that administration of telmisartan inhibits its pathologic, but not physiological, retinal neovascularization in a murine model of ischemic retinopathy, by prevention of

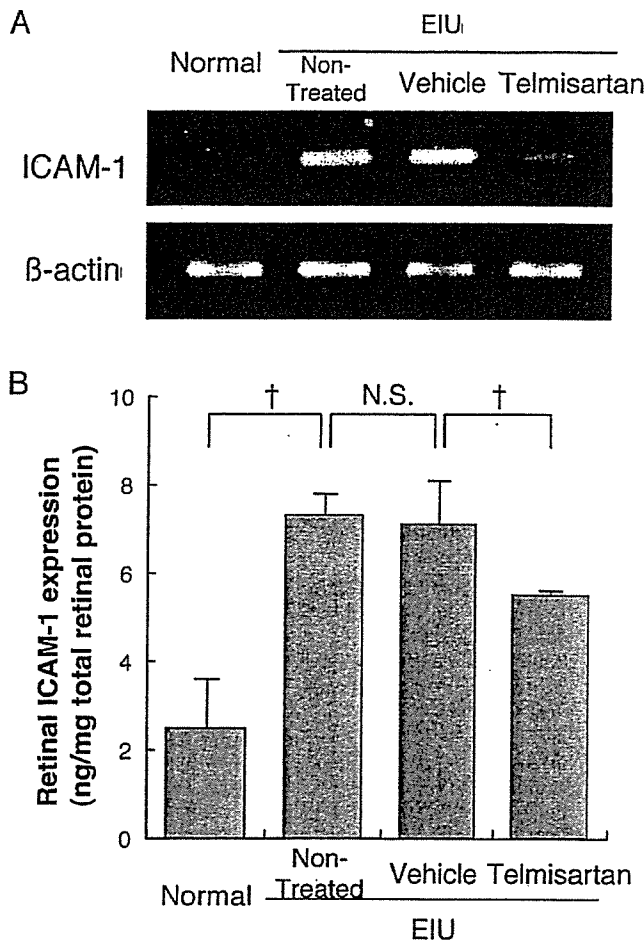


**FIGURE 3.** Effects of telmisartan on retinal ICAM-1 expression. RT-PCR (A) Retinal ICAM-1 mRNA expression in EIU mice treated with telmisartan was lower than that in nontreated and vehicle-treated EIU mice. Expression was very low in normal mice. (B) Retinal ICAM-1 protein levels in nontreated or vehicle-treated EIU mice were significantly higher than in normal mice and were significantly suppressed by treatment with telmisartan. The results represent the mean  $\pm$  SD;  $n = 6$ . † $P < 0.05$  by Mann-Whitney test.

ICAM-1-mediated leukocyte involvement in pathologic neovascularization.<sup>29</sup> The present data on EIU as a model of ocular inflammation more strictly confirm the anti-inflammatory effects of AT1-R blockade in the eye.

Besides ICAM-1, various chemical mediators are involved in the pathogenesis of EIU. In the present study, telmisartan treatment led to the suppression of EIU-induced cytokines including IL-6, TNF- $\alpha$ , COX-2, iNOS, and MCP-1. This result is compatible with those reported previously<sup>30,31</sup> demonstrating the inhibitory effects of AT1-R blockers on these inflammatory cytokines stimulated by LPS in other organs. The proinflammatory effects of angiotensin II are attributable to its induction of these inflammation-related molecules, most of which are downstream products of nuclear factor (NF)- $\kappa$ B, a transcription factor that promotes the gene expression of various inflammatory cytokines.<sup>32</sup> LPS-induced inflammation is mediated by the activation of NF- $\kappa$ B.<sup>32</sup> Indeed, ocular inflammation is suppressed by administration of an NF- $\kappa$ B inhibitor in EIU.<sup>33</sup> Taken together, the evidence shows that the anti-inflammatory effects of AT1-R blockers most likely result from suppressed gene expression of NF- $\kappa$ B-induced molecules. These previous findings, in accordance with our data, suggest that telmisartan

affects not only ICAM-1-mediated leukocyte adhesion but also various inflammatory processes.

In the present study, although anterior-chamber cell infiltration was substantially suppressed by telmisartan, little or no significant change was detected in protein leakage. A similar discrepancy between cell infiltration and protein leakage was also noted in several EIU studies by using neutralizing antibodies against ICAM-1, E-selectin,<sup>34</sup> P-selectin,<sup>34</sup> LFA-1,<sup>9,10</sup> and IL-10.<sup>35</sup> Considering that prostaglandin E2, an inflammatory mediator in addition to the adhesion molecules, is operative in protein leakage<sup>36</sup> and that combined inhibition of both L- and P-selectin suppresses protein leakage,<sup>12,34</sup> the cell-protein discrepancy observed in the present and previous studies is most likely attributable to differential mechanisms controlling the multiple inflammatory phases.

Recent reports have revealed that the renin-angiotensin system plays central roles in pathologic vascular conditions including inflammation, angiogenesis, and vascular remodeling.<sup>15-20</sup> The renin-angiotensin system has been shown to exist locally in various organs and to promote inflammation-related pathogenesis in atherosclerosis,<sup>37</sup> cerebral infarction,<sup>38</sup> and pancreatitis.<sup>39</sup> AT1-R blockers other than telmisartan are also reported to be anti-inflammatory.<sup>37-39</sup> These recent findings suggest the possibility of AT1-R blockade as a therapeutic strategy for these disorders characterized by inflammation. In atherosclerosis, in which angiotensin II promotes the infiltration of monocytes and T lymphocytes, AT1-R blockade with irbesartan suppresses the expression of MCP-1 and subsequent macrophage infiltration.<sup>37</sup> In spontaneously hypertensive rats,

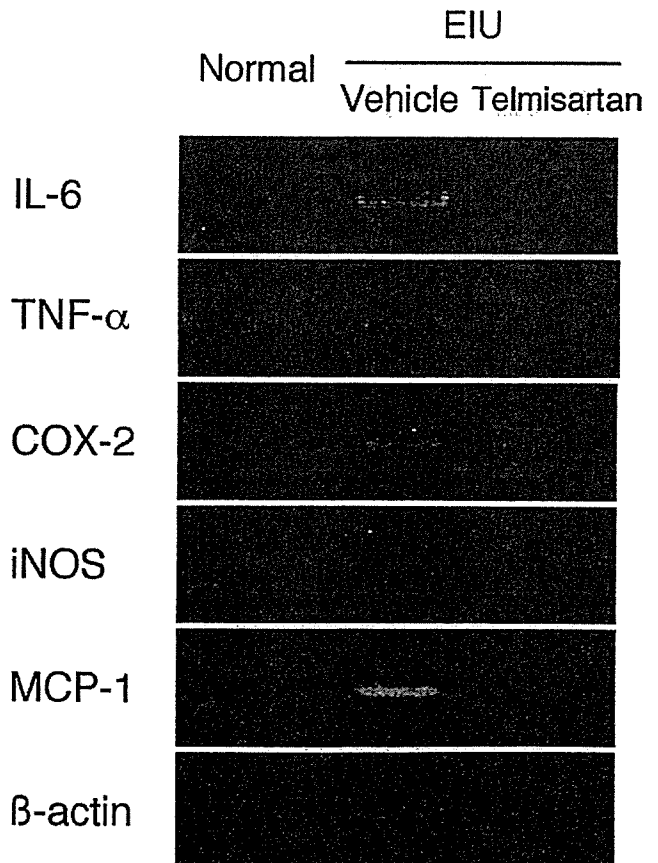


**FIGURE 4.** Effects of telmisartan on retinal expression of inflammatory mediators. Retinal mRNA expression of IL-6, TNF- $\alpha$ , COX-2, iNOS, and MCP-1 in vehicle-treated EIU mice was higher than in normal, age-matched mice and was suppressed by the administration of telmisartan.

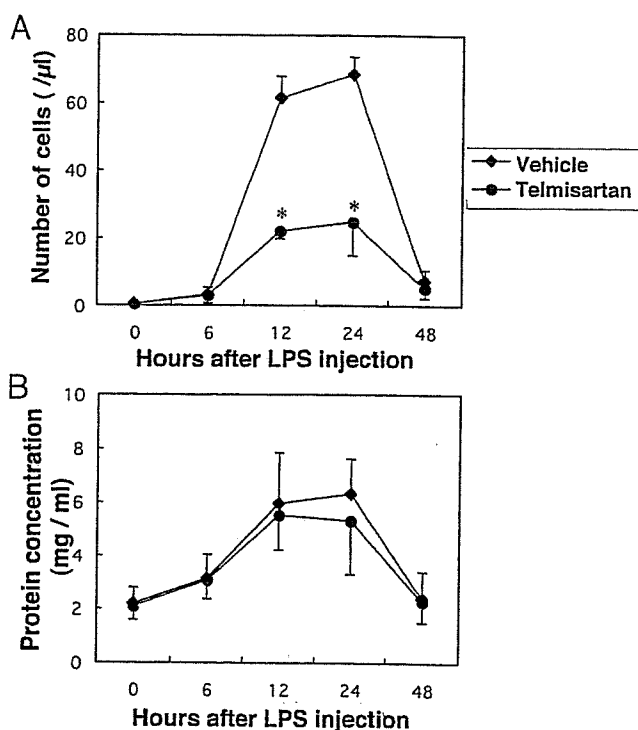


**FIGURE 5.** Effects of telmisartan on anterior uveitis. (A) The number of cells in aqueous humor 12 and 24 hours after LPS injection was markedly reduced by treatment with telmisartan. (B) The protein concentration in aqueous humor was not significantly suppressed by the treatment with telmisartan. ( $\blacklozenge$ ) Vehicle-treated and ( $\bullet$ ) telmisartan-treated mice. The results represent the mean  $\pm$  SD;  $n = 15$ . \* $P < 0.01$  by Mann-Whitney test.

which are vulnerable to brain ischemia, AT1-R blockade with candesartan suppresses ICAM-1-dependent leukocyte adhesion to the cerebral vessels, protecting against brain ischemia.<sup>38</sup> In acute pancreatitis, AT1-R blockade with losartan suppresses the production of reactive oxygen species by NADPH oxidase and reduces the severity of inflammation.<sup>39</sup> In addition, an angiotensin-converting enzyme inhibitor, widely used as an anti-hypertensive drug, is also reported to suppress vascular inflammation.<sup>40</sup> In the eye, localization of the renin-angiotensin system has been demonstrated without elucidation of its function,<sup>41,42</sup> except the possibility of an intraocular pressure modulator.<sup>42</sup> In the present study, AT1-R mRNA and protein expression is shown to be upregulated during the development of EIU. Further, AT1-R blockade suppressed ICAM-1-mediated leukocyte adhesion and infiltration. These results, in accordance with the previous data on inflammation in other organs, suggest the involvement of the renin-angiotensin system in ocular inflammation.

Currently, ocular inflammation such as chronic endogenous uveitis, is treated mainly with topical and/or systemic application of corticosteroids. During the long-term treatment with corticosteroids, however, care must be taken to guard against both ocular and systemic complications, including cataract, glaucoma, diabetes, hypertension, and osteoporosis. Clinically, AT1-R antagonists are widely and safely used in hypertensive patients. Combined with corticosteroid therapy, the anti-inflammatory effects of AT1-R blockade may benefit patients with chronic uveitis to decrease the rate and degree of the corticosteroid-induced complications. The present study is the first to indicate the potential use of AT1-R antagonists as a novel therapeutic strategy to suppress ocular inflammation.

## References

- Rosenbaum JT, McDevitt HO, Guss RB, Egbert PR. Endotoxin-induced uveitis in rats as a model for human disease. *Nature*. 1980;286:611-613.
- Bhattacharjee P, Williams RN, Eakins KE. An evaluation of ocular inflammation following the injection of bacterial endotoxin into the rat foot pad. *Invest Ophthalmol Vis Sci*. 1983;24:196-202.
- Hoekzema R, Verhagen C, van Haren M, Kijlstra A. Endotoxin-induced uveitis in the rat: the significance of intraocular interleukin-6. *Invest Ophthalmol Vis Sci*. 1992;33:532-539.
- Ohta K, Kikuchi T, Miyahara T, Yoshimura N. DNA microarray analysis of gene expression in iris and ciliary body of rat eyes with endotoxin-induced uveitis. *Exp Eye Res*. 2005;80:401-412.
- Koizumi K, Poulaki V, Doehmen S, et al. Contribution of TNF-alpha to leukocyte adhesion, vascular leakage, and apoptotic cell death in endotoxin-induced uveitis in vivo. *Invest Ophthalmol Vis Sci*. 2003;44:2184-2191.
- Bellot JL, Palmero M, Garcia-Cabanes C, Espi R, Hariton C, Orts A. Additive effect of nitric oxide and prostaglandin-E2 synthesis inhibitors in endotoxin-induced uveitis in the rabbit. *Inflamm Res*. 1996;45:203-208.
- Mo JS, Matsukawa A, Ohkawara S, Yoshinaga M. Role and regulation of IL-8 and MCP-1 in LPS-induced uveitis in rabbits. *Exp Eye Res*. 1999;68:333-340.
- Springer TA. Signals on endothelium for lymphocyte recirculation and leukocyte emigration: the area code paradigm. *Harvey Lect*. 1993-94;89:53-103.
- Becker MD, Garman K, Whitcup SM, Planck SR, Rosenbaum JT. Inhibition of leukocyte sticking and infiltration, but not rolling, by antibodies to ICAM-1 and LFA-1 in murine endotoxin-induced uveitis. *Invest Ophthalmol Vis Sci*. 2001;42:2563-2566.
- Whitcup SM, DeBarge LR, Rosen H, Nussenblatt RB, Chan CC. Monoclonal antibody against CD11b/CD18 inhibits endotoxin-induced uveitis. *Invest Ophthalmol Vis Sci*. 1993;34:673-681.
- Miyamoto K, Ogura Y, Hamada M, Nishiwaki H, Hiroshiba N, Honda Y. In vivo quantification of leukocyte behavior in the retina during endotoxin-induced uveitis. *Invest Ophthalmol Vis Sci*. 1996;37:2708-2715.
- Yamashiro K, Kiryu J, Tsujikawa A, et al. Suppressive effects of selectin inhibitor SKK-60060 on the leukocyte infiltration during endotoxin induced uveitis. *Br J Ophthalmol*. 2003;87:476-480.
- de Gasparo M, Catt KJ, Inagami T, Wright JW, Unger T. International union of pharmacology. XXIII. The angiotensin II receptors. *Pharmacol Rev*. 2000;52:415-472.
- Murphy TJ, Alexander RW, Griendling KK, Runge MS, Bernstein KE. Isolation of a cDNA encoding the vascular type-1 angiotensin II receptor. *Nature*. 1991;351:233-236.
- Tamarat R, Silvestre JS, Durie M, Levy BI. Angiotensin II angiogenic effect in vivo involves vascular endothelial growth factor and inflammation-related pathways. *Lab Invest*. 2002;82:747-756.
- Moravski CJ, Kelly DJ, Cooper ME, et al. Retinal neovascularization is prevented by blockade of the renin-angiotensin system. *Hypertension*. 2000;36:1099-1104.
- Chua CC, Hamdy RC, Chua BH. Upregulation of vascular endothelial growth factor by angiotensin II in rat heart endothelial cells. *Biochim Biophys Acta*. 1998;1401:187-194.
- Candido R, Allen TJ, Lassila M, et al. Irbesartan but not amlodipine suppresses diabetes-associated atherosclerosis. *Circulation*. 2004;109:1536-1542.
- Pastore L, Tessitore A, Martinotti S, et al. Angiotensin II stimulates intercellular adhesion molecule-1 (ICAM-1) expression by human vascular endothelial cells and increases soluble ICAM-1 release in vivo. *Circulation*. 1999;100:1646-1652.
- Okamura A, Rakugi H, Ohishi M, et al. Upregulation of renin-angiotensin system during differentiation of monocytes to macrophages. *J Hypertens*. 1999;17:537-545.
- Ohta K, Kikuchi T, Arai S, Yoshida N, Sato A, Yoshimura N. Protective role of heme oxygenase-1 against endotoxin-induced uveitis in rats. *Exp Eye Res*. 2003;77:665-673.
- Shiratori K, Ohgami K, Ilieva IB, Koyama Y, Yoshida K, Ohno S. Inhibition of endotoxin-induced uveitis and potentiation of cyclo-

- oxygenase-2 protein expression by alpha-melanocyte-stimulating hormone. *Invest Ophthalmol Vis Sci.* 2004;45:159-164.
23. Ohgami K, Ilieva I, Shiratori K, et al. Anti-inflammatory effects of aronia extract on rat endotoxin-induced uveitis. *Invest Ophthalmol Vis Sci.* 2005;46:275-281.
  24. Mandai M, Yoshimura N, Yoshida M, Iwaki M, Honda Y. The role of nitric oxide synthase in endotoxin-induced uveitis: effects of N<sup>G</sup>-nitro L-arginine. *Invest Ophthalmol Vis Sci.* 1994;35:3673-3680.
  25. Balt JC, Mathy MJ, Pfaffendorf M, van Zwieten PA. I Inhibition of angiotensin II-induced facilitation of sympathetic neurotransmission in the pithed rat: a comparison between losartan, irbesartan, telmisartan, and captopril. *J Hypertens.* 2001;19:465-473.
  26. Smith LE, Wesolowski E, McLellan A, et al. Oxygen-induced retinopathy in the mouse. *Invest Ophthalmol Vis Sci.* 1994;35:101-111.
  27. Baatz H, Puchta J, Reszka R, Pleyer U. Macrophage depletion prevents leukocyte adhesion and disease induction in experimental melanin-protein induced uveitis. *Exp Eye Res.* 2001;73:101-109.
  28. Cheng ZJ, Vaskonen T, Tikkanen I, et al. Endothelial dysfunction and salt-sensitive hypertension in spontaneously diabetic Goto-Kakizaki rats. *Hypertension.* 2001;37:433-439.
  29. Nagai N, Noda K, Urano T, et al. Selective suppression of pathological, but not physiological, retinal neovascularization by blocking angiotensin II type 1 receptor. *Invest Ophthalmol Vis Sci.* 2005;46:1078-1084.
  30. Niimi R, Nakamura A, Yanagawa Y. Suppression of endotoxin-induced renal tumor necrosis factor-alpha and interleukin-6 mRNA by renin-angiotensin system inhibitors. *Jpn J Pharmacol.* 2002;88:139-145.
  31. Lee HY, Noh HJ, Gang JG, et al. Inducible nitric oxide synthase (iNOS) expression is increased in lipopolysaccharide (LPS)-stimulated diabetic rat glomeruli: effect of ACE inhibitor and angiotensin II receptor blocker. *Yonsei Med J.* 2002;43:183-192.
  32. Baeuerle PA, Henkel T. Function and activation of NF-kappa B in the immune system. *Annu Rev Immunol.* 1994;12:141-179.
  33. Ohta K, Nakayama K, Kurokawa T, Kikuchi T, Yoshimura N. Inhibitory effects of pyrrolidine dithiocarbamate on endotoxin-induced uveitis in Lewis rats. *Invest Ophthalmol Vis Sci.* 2002;43:744-750.
  34. Suzuma I, Mandai M, Suzuma K, Ishida K, Tojo SJ, Honda Y. Contribution of E-selectin to cellular infiltration during endotoxin-induced uveitis. *Invest Ophthalmol Vis Sci.* 1998;39:1620-1630.
  35. Hayashi S, Guecx-Crosier Y, Delvaux A, Velu T, Roberge FG. Interleukin 10 inhibits inflammatory cells infiltration in endotoxin-induced uveitis. *Graefes Arch Clin Exp Ophthalmol.* 1996;234:633-636.
  36. Herbert CP, Okumura A, Mochizuki M. Endotoxin-induced uveitis in the rat: a study of the role of inflammation mediators. *Graefes Arch Clin Exp Ophthalmol.* 1988;226:553-558.
  37. Dol F, Martin G, Staels B, et al. Angiotensin AT1 receptor antagonist irbesartan decreases lesion size, chemokine expression, and macrophage accumulation in apolipoprotein E-deficient mice. *J Cardiovasc Pharmacol.* 2001;38:395-405.
  38. Ando H, Zhou J, Macova M, Imboden H, Saavedra JM. Angiotensin II AT1 receptor blockade reverses pathological hypertrophy and inflammation in brain microvessels of spontaneously hypertensive rats. *Stroke.* 2004;35:1726-1731.
  39. Tsang SW, Ip SP, Leung PS. Prophylactic and therapeutic treatments with AT 1 and AT 2 receptor antagonists and their effects on changes in the severity of pancreatitis. *Int J Biochem Cell Biol.* 2004;36:330-339.
  40. da Cunha V, Tham DM, Martin-McNulty B, et al. Enalapril attenuates angiotensin II-induced atherosclerosis and vascular inflammation. *Atherosclerosis.* 2005;178:9-17.
  41. Wagner J, Jan Danser AH, Derckx FH, et al. Demonstration of renin mRNA, angiotensinogen mRNA, and angiotensin converting enzyme mRNA expression in the human eye: evidence for an intraocular renin-angiotensin system. *Br J Ophthalmol.* 1996;80:159-163.
  42. Cullinane AB, Leung PS, Ortego J, Coca-Prados M, Harvey BJ. Renin-angiotensin system expression and secretory function in cultured human ciliary body non-pigmented epithelium. *Br J Ophthalmol.* 2002;86:676-683.

# Discordance Between Subjective Perimetric Visual Fields and Objective Multifocal Visual Evoked Potential-Determined Visual Fields in Patients With Hemianopsia

KEN WATANABE, MD, KEI SHINODA, MD, ITARU KIMURA, MD,  
YUKIHIKO MASHIMA, MD, YOSHIHISA OGUCHI, MD, AND HISAO OHDE, MD

- **PURPOSE:** To investigate the concordance between subjectively and objectively acquired visual fields in patients with subjectively determined hemianopsia.
- **DESIGN:** Retrospective observational study.
- **METHODS:** Ten patients, six men and four women, ranging in age from 28 to 68 years, were studied. Goldmann or Humphrey perimeters were used to obtain the subjectively determined visual fields for up to 25 degrees of eccentricity, and the VERIS Scientific System (Electro-Diagnostic Imaging, San Francisco, California, USA) was used to record multifocal visual evoked potential [VEPs] (mfVEPs) to obtain the objective visual fields. Each of the 60 black-and-white segments of the checkerboard stimulus was alternated according to a binary m sequence. The first slices of the second-order kernels were extracted and analyzed.
- **RESULTS:** In five cases, the visual field loci where the mfVEPs were within normal limits corresponded to the scotomatous areas obtained by conventional perimetry. In these discordant cases, the lesions (e.g., arteriovenous malformation) were located in the occipital lobe. Two of these cases had a complete recovery of the subjective visual field. The lesions of the concordant cases were located outside the occipital lobe (e.g., pituitary adenoma). In these cases, no visual field improvement was seen. The temporal crescent syndrome was ruled out in patients with posterior lesions by computed tomography (CT) or magnetic resonance imaging (MRI) findings.

- **CONCLUSIONS:** In some patients with occipital lesions, the subjective and objective visual field results are discordant, and some of them will show a recovery of the visual field deficits. (Am J Ophthalmol 2007;143:295–304. © 2007 by Elsevier Inc. All rights reserved.)

**V**ISUAL FIELDS OBTAINED BY THE GOLDMANN AND Humphrey perimeters have been the gold standards for the evaluation of optic nerve diseases and pathologic changes in the visual pathways. These tests are used routinely, but, unfortunately, they are subjective tests. Several methods have been used to try to determine the visual fields objectively; for example, conventional flash and pattern visual-evoked potentials (VEPs),<sup>1–5</sup> vector VEPs,<sup>6</sup> pupillography,<sup>7</sup> scalp topography of VEPs,<sup>8</sup> positron emission tomography,<sup>9</sup> multifocal VEPs (mfVEPs),<sup>10–19</sup> and functional magnetic resonance imaging (MRI).<sup>20–22</sup> However, none of these techniques is used routinely on patients.

The topographic map of the amplitudes of the mfVEPs has been reported to show good agreement or concordance with the results of conventional visual field tests if occipital bipolar electrodes are used.<sup>15,16</sup> Thus mfVEPs have been used on patients with glaucoma to evaluate the functional glaucomatous loss objectively.<sup>19,23,24</sup> In addition, the mfVEPs, summed within the four quadrants, have been used as an objective evaluator of the visual fields in patients with visual field loss.<sup>16,17,19,23,24</sup> However, we have found that the alterations of the topographic map of the mfVEPs are not always in good concordance with the subjectively determined visual fields in some cases with hemianopic field defects.

The purpose of this study was to determine whether the subjectively obtained visual fields and the objectively obtained visual fields were concordant in patients with hemianopsia. In addition, we examined whether the discordance of the subjective and objective visual fields was related to the location of the lesion giving rise to the hemianopsia.

AJO.com

Supplemental Material available at AJO.com.



















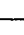

Accepted for publication Oct 16, 2006.

From the Department of Ophthalmology, Keio University School of Medicine (K.W., K.S., I.K., Y.M., Y.O., H.O.); Laboratory of Visual Physiology, National Institute of Sensory Organs, Tokyo Medical Center (K.S.); and Kamoshita Eye Clinic (H.O.), Tokyo, Japan.

Inquiries to Hisao Ohde, MD, Department of Ophthalmology, Keio University School of Medicine, 35 Shinanomachi, Shinjuku-ku, Tokyo 160-8582, Japan; e-mail: shinodakei@kankakuki.go.jp



**TABLE 1.** Demographics and Summary of the Findings of mfVEP and Diagnosis of the Patients

Patient No	Age	Gender	Visual Field Loss	Diagnosis	mfVEPs (Concordance or Not)
1	51	F	Btemp. h.  	Pituitary adenoma	Yes
2	49	M	Btemp. h.  	Pituitary adenoma	Yes
3	38	F	Rt. homo. h.  	Skull base meningioma	Yes
4	60	F	Lt. homo. h.  	Brain meta (rt. parieto-occipital)	Yes
5	49	M	Lt. homo. h.  	Craniopharyngioma	Yes
6	46	M	Rt. homo. h.  	Meningioma (lt. occipital)	No
7	28	M	Lt. homo. h.  	AVM postoperatively (rt. occipital)	No
8	68	M	Lt. homo. h.  	Glioma (rt. occipital)	No
9	35	M	Rt. homo. h.  	Cavernous hemangioma (lt. occipital)	No
10	30	F	Lt. homo. h.  	Subarachnoid hemorrhage postoperatively (rt. occipital)	No

mfVEP = multifocal visual evoked potentials; M = male; F = female; btemp. h = bitemporal hemianopsia; rt. homo. h = right homonymous hemianopsia; lt. = left; AVM = arteriovenous malformation.

Concordance or not: "yes" means that no mfVEP response was observed at the area of visual field deficit. "no" means that mfVEP response was observed at the area of visual field deficit.

## METHODS

• **SUBJECTS:** All of the research procedures conformed to the guidelines of the Declaration of Helsinki, and an informed consent was obtained from all subjects after an explanation of the purpose and the procedures to be used in the experiments. The mfVEPs were recorded from 10 consecutive patients who had hemianopsia, either a complete hemianopsia or quadrantanopsia, which was documented by conventional perimetry. The examinations were performed between January 1999 and February 2004 at the Keio University Hospital. The patients consisted of six men and four women whose ages ranged from 28 to 68 years with a mean of  $45.4 \pm 12.8$  years ( $\pm$  standard deviation [SD]; Table 1). Three of the patients had a right and five patients had a left homonymous hemianopsia. The two remaining patients had bitemporal hemianopsia. All patients had evidence of damage to the visual pathway by computed tomography (CT) or magnetic resonance imaging (MRI), or both, which could account for the visual field deficits. The causes of the visual impairment were brain tumors, cerebral infarctions, or postneurosurgery for either arteriovenous malformation or subarachnoid hemorrhage. The temporal crescent syndrome was ruled out in patients with posterior lesions by CT or MRI findings.

All patients had a routine ophthalmologic examination including slit-lamp biomicroscopy, ophthalmoscopy, and attenuation tonometry. All patients had a corrected visual acuity of 20/20 or better and a refractive error of less than  $-5.25$  diopters in both eyes. There was no history of ophthalmologic abnormalities such as glaucoma or diabetic retinopathy that could affect the visual function especially the visual fields. The perimetric examinations and mfVEPs recordings were carried out during the same period. Normative data were collected from 10 healthy eyes except for refractive

error, although the age did not match the patients (age range, 27 to 65;  $35.6 \pm 11.6$ ).

Because the SDs of the amplitudes of the multifocal electroretinograms (mfERGs) were relatively large (see Supplemental Table 1 available at AJO.com) in normal subjects, the ratio of the amplitudes or implicit times from horizontally adjacent quadrants was calculated. For example, the ratio of the amplitude of the summed response from superior nasal quadrant was compared with that from the superior temporal quadrant, the SN/ST ratio. The ratios of the amplitudes of the mfVEPs in the inferior nasal to inferior temporal ratio (IN/IT) were calculated in the same way. The SN/ST and IN/IT ratios of the implicit times were also calculated for R1 and R2. It was reported,<sup>16,24,25</sup> and confirmed here, that the general shape of the summed responses of the temporal and nasal visual fields are very similar, whereas those of the superior and inferior visual fields differed in phase and amplitude in normal subjects.

• **STIMULUS FOR MFVEPS:** The stimulus was similar to that used in Klistner protocol, with a dartboard pattern consisting of 61 sectors that was created on a computer monitor (17 inch, high-resolution display, stimulation rate 75 Hz; Nanao, Ishikawa, Japan).<sup>15</sup> Each check was either white or black with a 92% contrast (white =  $160 \text{ cd/m}^2$ ; black =  $7 \text{ cd/m}^2$ ), and the luminance alternated pseudorandomly at 75 frames per second. The m binary sequence was repeated two times.<sup>16</sup>

The individual kernels of the responses were determined by cross-correlating the digitized output signal with the binary input sequences using a fast Walsh transform. As shown in the Supplemental Figures 1 and 2 (available at AJO.com), the size of each segment was cortically scaled with eccentricity to stimulate approximately equal areas of cortical (striate) surface.<sup>15,18,26-29</sup> The overall stimulus subtended approximately 25 degrees at the eye.



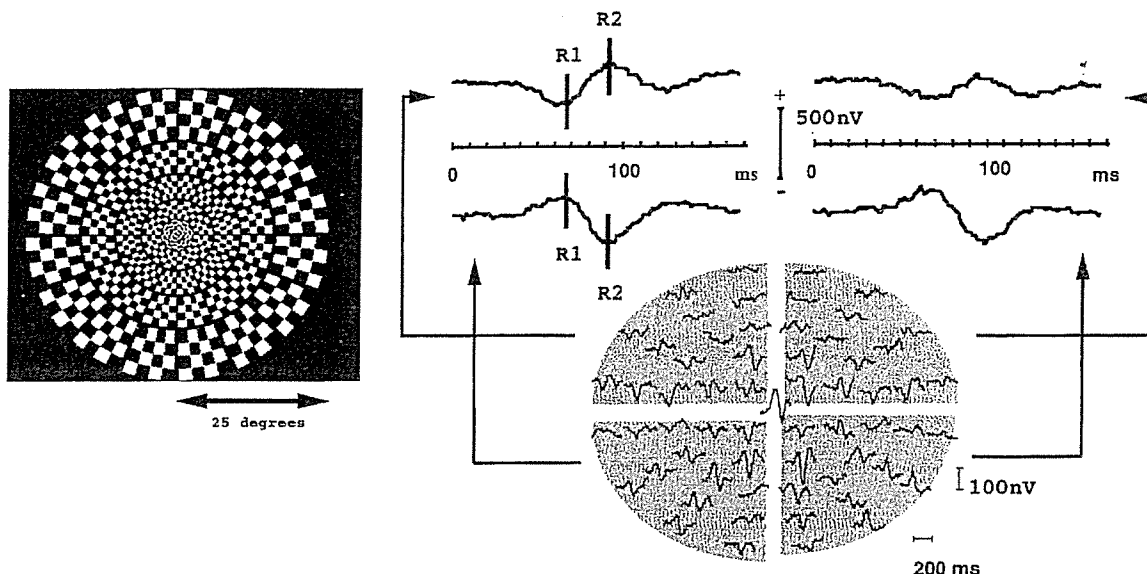


FIGURE 1. Stimulus for multifocal visual-evoked potentials. (Left) Stimulus was a dartboard pattern consisting of 61 sectors. (Right) Individual second-order kernels of the multifocal visual evoked potentials (mfVEPs) are plotted retinotopically in the lower half. The sums of the responses in each of the four quadrants are plotted in the sectors in the upper half except for the response from the very central sector.<sup>16</sup>

TABLE 2. The Ratio of the mfVEPs Parameters in All the Patients

Case	Conventional Left Eye	Visual Field Right Eye	Amplitude				R1 Latency				R2 Latency			
			Left Eye		Right Eye		Left Eye		Right Eye		Left Eye		Right Eye	
			SN/ST	IN/IT	SN/ST	IN/IT	SN/ST	IN/IT	SN/ST	IN/IT	SN/ST	IN/IT	SN/ST	IN/IT
No.1	⊙	⊙	—	—	—	—	—	—	—	—	—	—	—	—
No.2	⊙	⊙	—	1.829	—	1.652	—	0.989	—	0.956	—	1.074	—	0.945
No.3	⊙	⊙	—	—	—	—	—	—	—	—	—	—	—	—
No.4	⊙	⊙	—	—	—	—	—	—	—	—	—	—	—	—
No.5	⊙	⊙	—	—	—	—	—	—	—	—	—	—	—	—
No.6	⊙	⊙	0.618	1.792	1.630	0.485	1.244	1.000	0.939	1.449 H	0.955	0.945	0.875 L	1.479 H
No.7	⊙	⊙	1.750	0.821	0.604	1.400	1.000	0.868 L	1.211	1.024	1.171 H	0.914	1.325 H	1.268 H
No.8	⊙	⊙	1.130	0.612	0.374	1.732	0.977	0.878 L	0.951	1.084	1.038	0.863 L	1.000	1.135 H
No.9	⊙	⊙	0.731	1.771	1.226	0.868	1.057	1.325 H	1.524 H	1.439 H	1.044	1.549 H	1.171 H	1.009
No.10	⊙	⊙	0.980	1.786	0.803	0.462	0.988	0.976	1.000	1.000	0.975	1.102	0.911 L	1.027

P1 amplitude = amplitude of the first positive component around 100 ms after stimulation; R1 latency = time interval between the stimulation and first negative component around 75 ms after stimulation; R2 latency = time interval between the stimulation and first positive component around 100 ms after stimulation; SN = superior nasal; ST = superotemporal; IN = inferionasal; IT = inferiortemporal.

The ratio of each mfVEPs parameters in the normal control subjects are shown in the Supplemental Table.

The mean  $\pm 2^*$  SD were defined as cut-off values. When the patient's ratio of any mfVEPs parameter was out of this range, it is indicated with H or L in this Table. H = the value is higher than the cut-off value; L = the value is lower than the cut-off value; — = the ratio could not be calculated because the response from the quadrant of conventional visual field defect was noise level.

To rule out cross-talk, half of the dartboard stimulus field was covered and the mfVEPs were recorded as usual. The mfVEPs usually elicited from the covered loci were completely flat.<sup>30</sup>

• RECORDING MFVEPs: Patients were preadapted to standard room lighting, and all recordings were performed under

dim room lights. The pupils were fully dilated with 0.5% tropicamide and 0.5% phenylephrine hydrochloride. A small red fixation light was present in the center of the stimulus display, and the subjects were instructed to fixate on the red light and to try not to blink. The subjects wore their best refractive correction, and all recordings were monocular. One of the recording electrodes was placed 2.0 cm inferior to

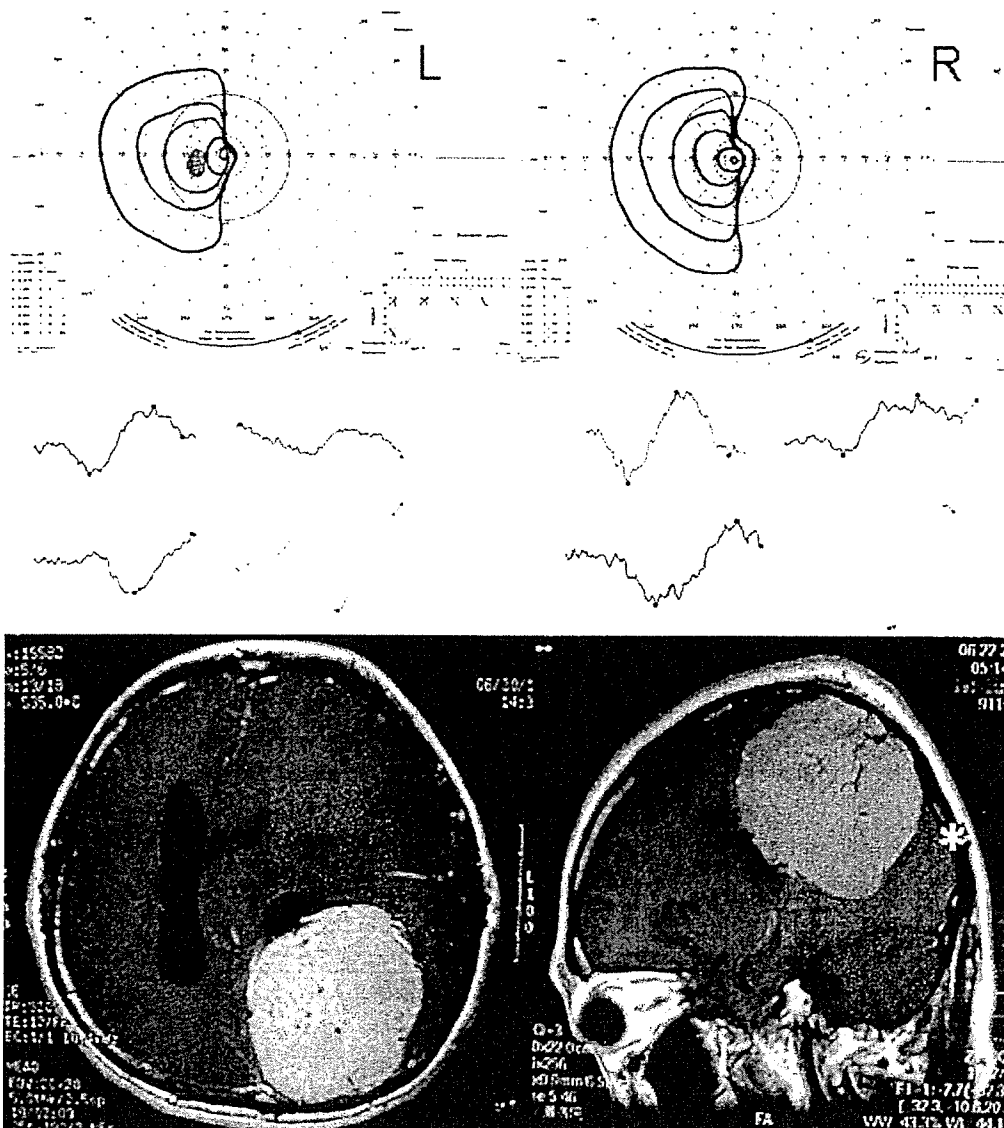


FIGURE 2. Findings in a 46-year-old man (Case 6) with right homonymous hemianopsia due to a meningioma extending from the left parietal lobe to the occipital lobe. (Top) Goldmann perimetric fields showing a left homonymous hemianopsia. (Middle) The multifocal visual evoked potentials (mfVEPs) are presented so that the average waveforms are seen in each of the quadrants where each waveform originates. The mfVEPs are not extinguished in the temporal fields of the right eye and the nasal fields of the left eye. (Bottom) An axial plane (left) and sagittal plane (right) of the magnetic resonance imaging (MRI) scan show a meningioma extending from the left parietal lobe to occipital lobe. Most of the lesion was primarily outside of primary visual cortex and in a more distal area.

(negative electrode) and the other 2.0 cm superior to (positive electrode) theinion.<sup>15,16,32</sup> The ground electrode was placed on the earlobe.

The mfVEPs were recorded with the VERIS II system (Tomey Co, Nagoya, Japan). Signals were amplified 50,000 times and bandpass filtered from 0.5 to 100 Hz. The sampling rate was 75 Hz, and the m-15 binary stimulation sequence was divided into 32 slightly overlapping segments. Each run was divided into eight equal segments with a total recording time of about seven minutes.

• **ANALYSES:** All of the mfERG data were analyzed using VERIS Science 3.01 software (Tomey Co, Nagoya, Japan).<sup>16</sup> The first slice of the second-order kernel was extracted and

the 60 responses (omitting the central response) were divided into four quadrants and summed. Each mfVEP consisted of the R1 and R2 components that probably correspond to the N70 and P100 components of conventional VEPs (Figure 1). The implicit times and amplitudes (R2 peak – R1 peak) of R1 and R2 were calculated.

If the response of the mfVEPs was reduced in the area where an absolute scotoma was detected by conventional visual field testing, this case was considered to have a concordance between the subjective and objective visual fields. To judge whether the amplitude from the quadrant was normal, we used a criterion of <2 SDs from the same region in normal subjects (see Supplemental Table 2 available at AJO.com).

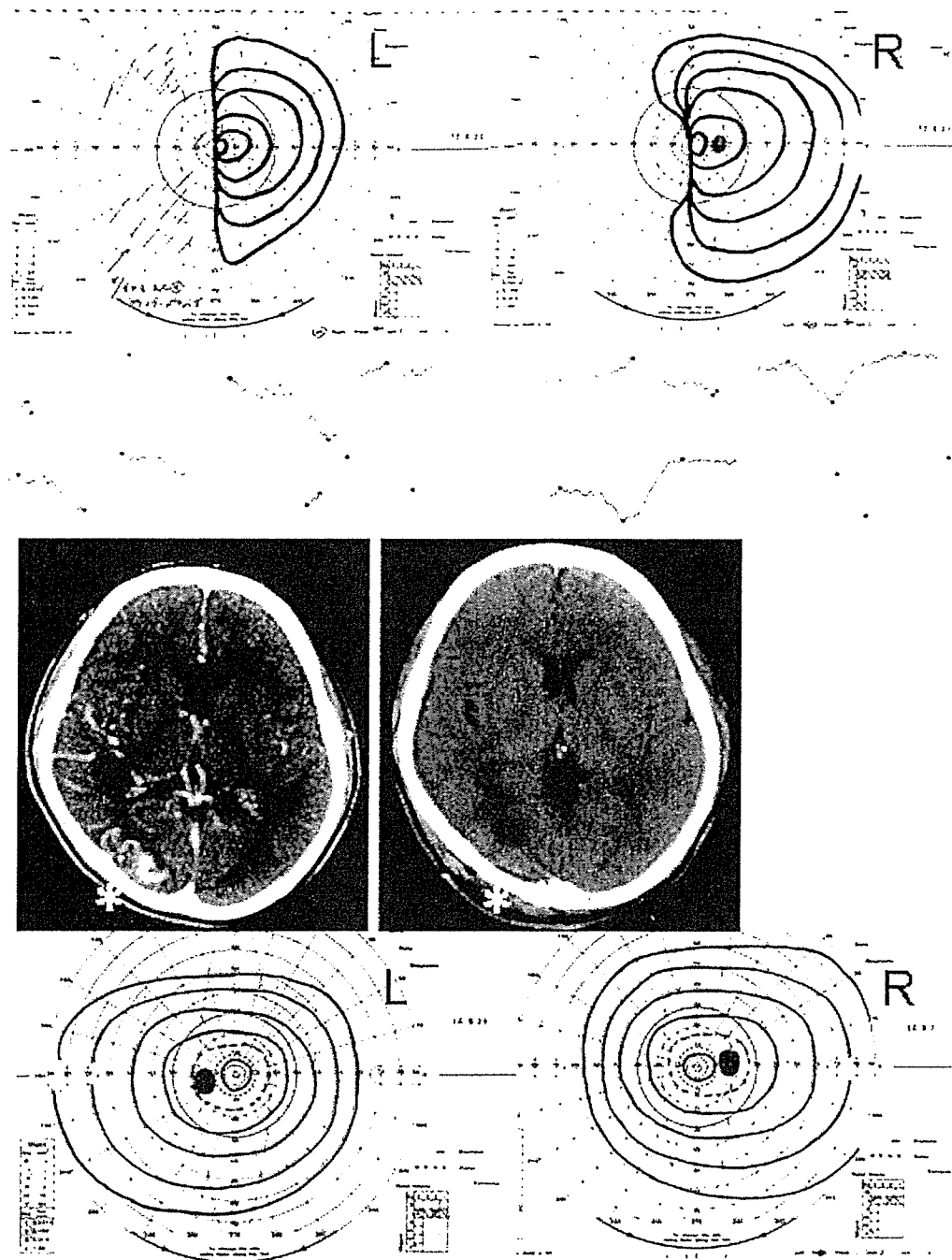


FIGURE 3. Findings in a 28-year-old man (Case 7) who underwent neurosurgery for an arteriovenous malformation in the right occipital lobe. (Top) Goldmann visual fields showing a left homonymous hemianopsia. (Second row) The multifocal visual evoked potentials (mfVEPs) are presented so that the average waveforms are seen in each of the quadrants where in the visual field each waveform originates. The mfVEPs were not extinguished in the temporal fields of the left eye and the nasal fields of the right eye. (Third row, left) Computed tomographic (CT) image showing an arteriovenous malformation in the right occipital lobe. (Third row, right) CT image showing a low-density area indicating postoperative edema in the right occipital region. (Bottom) Goldmann perimetric fields showing complete recovery of visual fields three months later.

## RESULTS

THE SHAPES OF THE SUMMED MFVEPS IN THE UPPER visual field were approximately a mirror image of those in the lower field in normal subjects. This was also true for the mfVEPs elicited from the nonaffected quadrants of the patients.<sup>16</sup> The ratio of the mfVEPs parameters in all the

patients are shown in Table 1. In some cases, the ratio could not be calculated because the mfVEP was at noise level.

A summary of our findings in the 10 cases is presented in Table 2. Five of 10 patients showed good concordance between the subjective and the objective visual fields. Thus the amplitudes of the mfVEPs were within

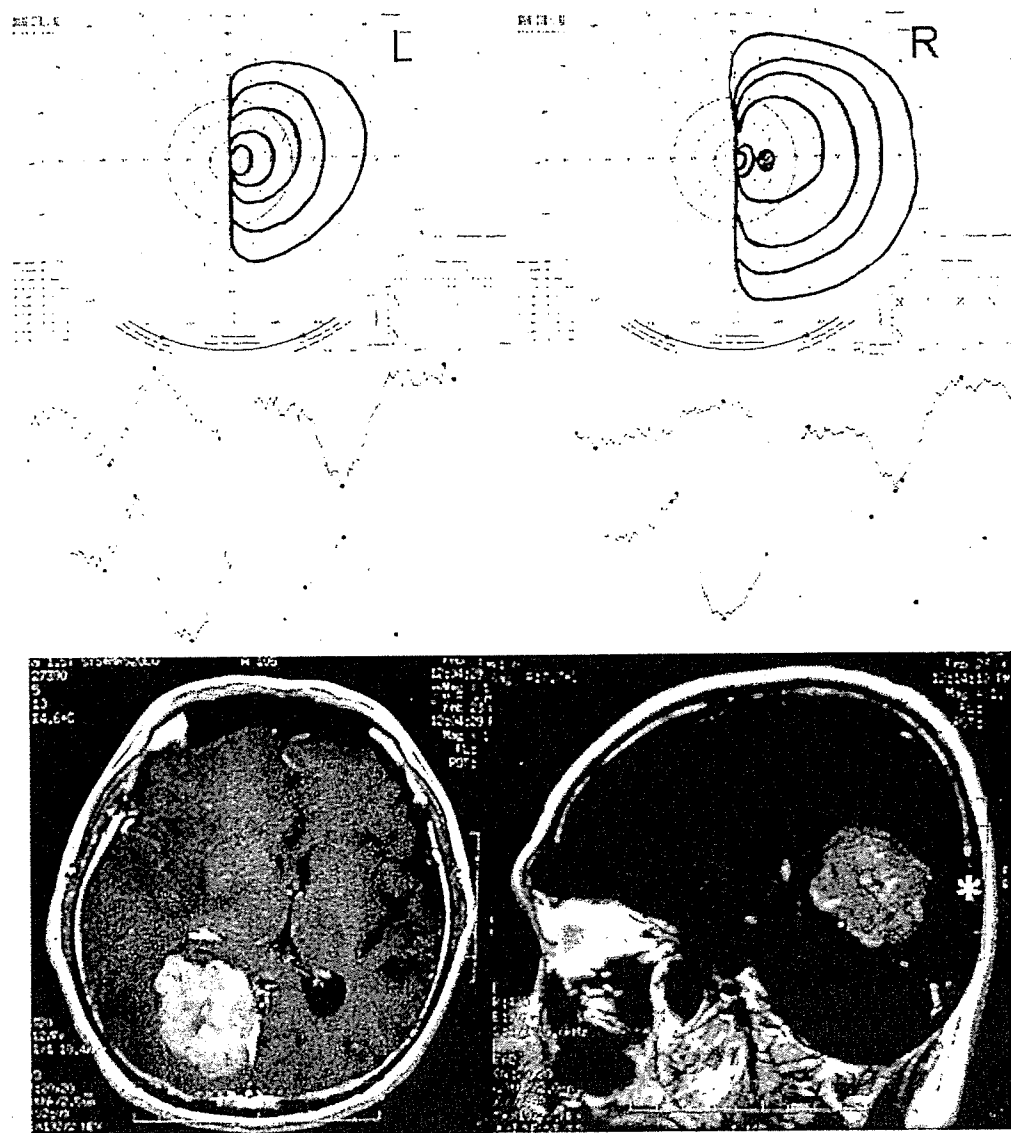


FIGURE 4. Findings in a 68-year-old man (Case 8) who complained of visual loss in his left field and was found to have a glioma in the right occipital lobe. (Top) Goldmann perimetric fields showing a left homonymous hemianopsia. (Middle) The multifocal visual-evoked potentials (mfVEPs) are presented so that the average waveforms are seen in each of the quadrants where in the visual field each waveform originates. The mfVEPs have relatively good responses in the temporal fields of the left eye and the nasal fields of the right eye. (Bottom) An axial plane (left) and sagittal plane (right) of the magnetic resonance imaging (MRI) scan revealed a mass about  $5 \times 5$  cm in the right occipital lobe, which was diagnosed as a glioma. Most of the lesion was primarily outside the primary visual cortex and in more distal areas.

normal limits in each quadrant in which the visual field was normal by conventional perimetry, and either the amplitude was reduced or the implicit time was delayed in the quadrants corresponding to the visual field deficits detected by perimetry. The visual field defects in these cases were due to a brain lesion outside the occipital cortex.

In contrast, the results of conventional perimetry and mfVEP topographic analysis in the other five cases were discordant. In these five patients, normal or only slightly reduced mfVEPs were recorded in the quadrants from which a subjective visual field deficit was detected. Interestingly in these cases, the site of the lesion was found in the occipital cortex in all five patients. Two of these cases

(Cases 7 and 10) had a complete recovery of their visual field after the cause of the brain lesion was treated or in remission. In the five cases (Cases 1 through 5) in which the results from mfVEP were concordant with the subjective visual fields, there was no recovery of the visual fields determined by conventional perimetry.

- **CASE 6:** A 46-year-old man with a right homonymous hemianopsia from a meningioma. The ratios of the amplitude of the mfVEPs for SN/ST and IN/IT in the right eye were 0.618 and 1.792, respectively, whereas the normal ranges (mean  $\pm$  2 SD) were 0.311 to 1.763 and 0.155 to 1.85, respectively (Figure 2, Table 2). The ratios for SN/ST and IN/IT in the left eye were 1.630 and 0.485, respec-

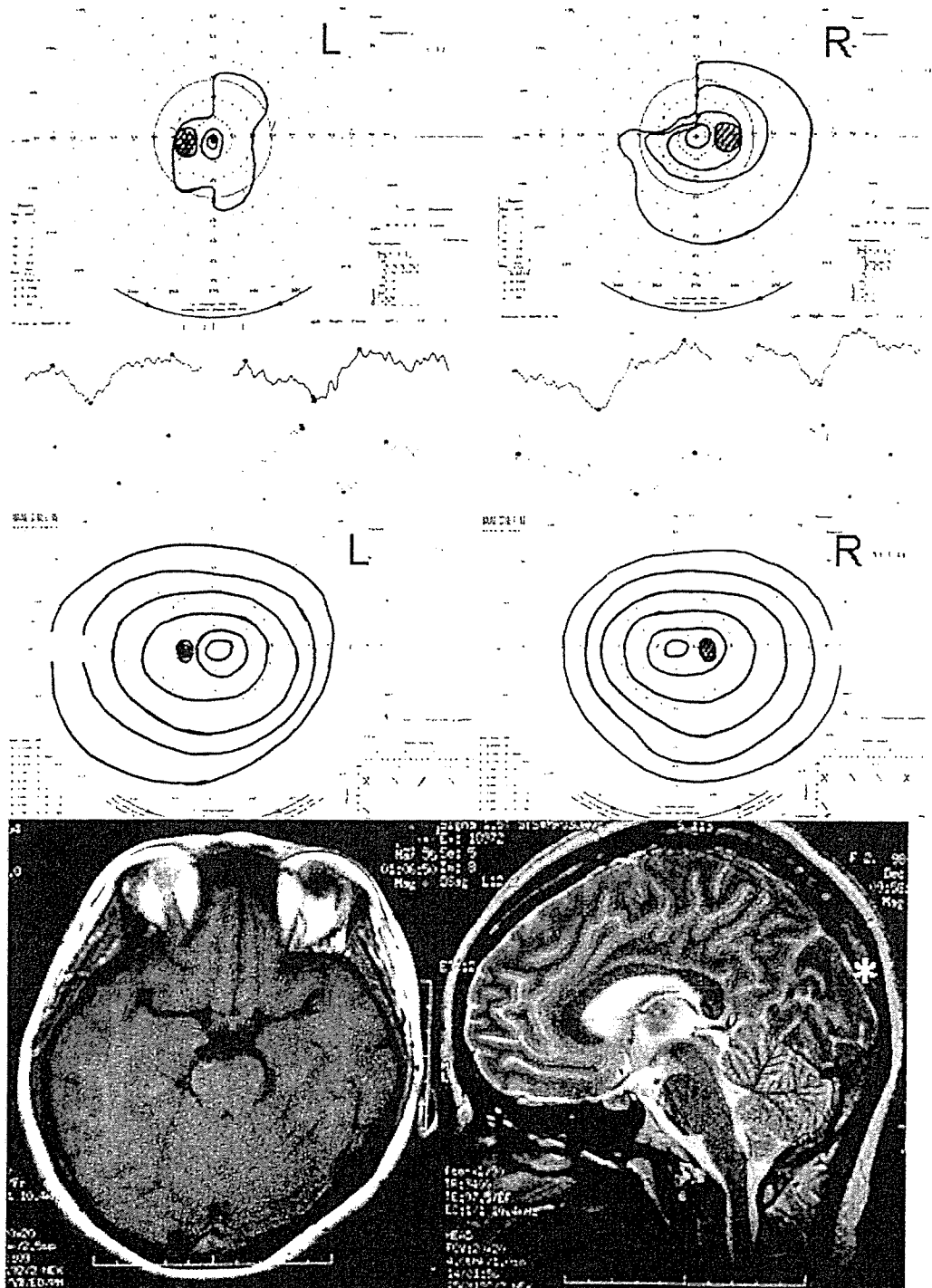


FIGURE 5. Findings in a 30-year-old-woman (Case 10) who underwent neurosurgery for subarachnoidal hemorrhage in the right occipital lobe resulting from an aneurysm of the posterior communicating artery. She complained of a visual field loss in the left field two months after surgery. (Top) Goldmann perimetric fields showing a left homonymous hemianopsia. (Second row) The multifocal visual evoked potentials (mfVEPs) are presented so that the average waveforms are seen in each of the quadrants where in the visual field each waveform originates. The mfVEPs demonstrated good responses in the nasal superior field of both eyes. (Third row) Three months later, the Goldmann fields demonstrate a complete recovery of the visual field. (Bottom right) An axial plane (left) and sagittal plane (right) of the magnetic resonance imaging (MRI) scan revealed neither particular edema nor infarction.

tively. All of these ratios were within the normal limits, suggesting that the mfVEPs were not altered in the temporal fields of the right eye and the nasal fields of the left eye. Therefore, his subjectively and objectively determined visual fields were discordant (Figure 2). His cor-

rected visual acuity was 20/20 in both eyes, and Goldmann perimetry showed a right homonymous hemianopsia with foveal sparing. An MRI scan demonstrated a mass extending from the left parietal lobe to the occipital lobe, which was diagnosed as a meningioma.

• **CASE 7:** A 28-year-old man underwent surgery for an arteriovenous malformation in the right occipital lobe, and had homonymous hemianopsia postoperatively (Figure 3). The neurosurgeon referred the patient to our department for visual field examination. Examination revealed a corrected visual acuity of 20/20 in each eye, and Goldmann perimetry demonstrated a left homonymous hemianopsia. The ratios of the amplitudes of the mfVEPs for SN/ST and IN/IT in the right eye were 1.750 and 0.821, respectively (Table 2). The ratios for the left eye were 0.604 and 1.400, respectively (Table 2). All of the ratios were within the normal limits, suggesting that the mfVEPs were not altered the temporal fields of the left eye and the nasal fields of the right eye (i.e., a discordance).

Preoperative CT scan showed a nidus of about  $2 \times 2$  cm on the right occipital lobe. CT scans seven days after the operation showed a low-density area that appeared to be postoperative edema. Goldmann perimetry showed a complete recovery of the visual fields three months after the operation.

• **CASE 8:** A 68-year-old man who had left homonymous hemianopsia from a glioma. The ratios of the amplitudes of the mfVEPs for SN/ST and IN/IT in the right eye were 1.130 and 0.612, respectively (Figure 4, Table 2). The same ratios for the left eye were 0.374 and 1.732, respectively. The ratios of the mfVEPs were within normal limits in the temporal field of the left eye and the nasal field of the right eye. His corrected visual acuity was 20/20 in each eye, and Goldmann perimetry showed a left homonymous hemianopsia. Therefore, his subjectively and objectively determined visual fields were concordant (Figure 4). An MRI scan revealed a mass about  $5 \times 5$  cm in the right occipital lobe, which was diagnosed as a glioma.

• **CASE 10:** A 30-year-old woman who complained of a visual loss in the left field two months after neurosurgery for a subarachnoidal hemorrhage in the right occipital lobe resulting from an aneurysm in the posterior communicating artery. The neurosurgery caused a stenosis of the posterior cerebral artery. The ratios of the amplitudes of the mfVEPs for SN/ST and IN/IT in the right eye were 0.980 and 1.786, respectively. These findings indicate that the mfVEPs were not altered in the right eye even in the superior nasal visual field (Figure 5, Table 2). The ratios of the amplitude in the left eye were 0.803 and 0.462, respectively. The Goldmann visual field of the left eye showed reduced sensitivities in all the quadrants. The mfVEP amplitude for each quadrant was normal. She had a left homonymous hemianopsia with reduced sensitivities in the left eye postoperatively that showed discordance in both eyes (Figure 5). Her corrected visual acuity was 20/20 in each eye. Goldmann perimeter showed a left homonymous hemianopsia and concentric visual field deficit in the left eye. An MRI scan revealed neither edema nor infarc-

tion. Five months later, Goldmann perimetry demonstrated a complete recovery of the visual fields.

## DISCUSSION

WE HAVE EVALUATED THE MFVEPS RECORDED WITH BIPOLAR occipital electrodes that straddled theinion and were elicited by a pseudorandom binary m sequence.<sup>16</sup> Our earlier results with the same stimulus and recording protocols showed that the summed mfVEPs in the four quadrants were highly concordant with the results of conventional subjective perimetry. Therefore, we concluded that this technique can be used to assess the visual field defects objectively in patients with diseases in the visual pathway.

However, as the number of such patients increased, we encountered some cases in which the mfVEPs were less impaired or even within normal limits in spite of visual field defects detected by conventional perimetry. We found that these discordant cases always had a lesion in the occipital area. However, the patients with homonymous hemianopsia from an occipital lesion did not always show such disagreement between subjective and objective visual fields.

The origin of human visual evoked potentials has been extensively investigated, and the evidence suggest that they originate from some part of the striate cortex or calcarine fissure.<sup>14,15,26,32-34</sup> Although the exact origin of the mfVEPs is still undetermined, they are believed to be mainly derived from area V1 of the striate cortex.<sup>35-38</sup> Therefore, mfVEPs and subjective visual field should be impaired from pathologic lesions in this area. If any part of the visual pathway before V1 is involved, the mfVEP recorded should be abnormal in the quadrants corresponding to the visual field defects, as seen in cases 1 and 2 in which chiasmal lesion led to bitemporal hemianopsia. In case 3, with a meningioma at the base of the skull, the mfVEPs were reduced in agreement with the homonymous left hemianopsia detected by Goldmann perimetry. This concordance can be reasonably explained by the postchiasmal damage of the visual pathway before V1.

However, localized damage of higher visual centers (e.g., V2/V3) can cause visual field defects when determined by perimetry but not by mfVEPs. We suggest that the discordance between the subjectively and objectively determined visual fields observed in the five cases was because the lesion was in the post-striate cortex. In the two cases (Cases 7 and 10) that had significant improvements of the visual field after a resolution of the brain lesion, we suggest that the postsurgical edema (Case 7) was the cause of the early visual field defect.

Klistner and associates recorded normal mfVEPs in patients with quadrantanopia that were consistent with an extrasubstrate lesion that was very congruous, complete, and respected the horizontal meridian. They stated that

mfVEPs are generated in the striate cortex (V1), and that topographic analysis of mfVEPs may be able to distinguish striate from extrastriate lesions.<sup>17</sup> Recently, a patient was reported with a congruous quadrantic defect and a loss of the fMRI signal in the corresponding extrastriate area, with normal signals in V1.<sup>21</sup>

Some investigators<sup>1-5,39-44</sup> have successfully recorded VEPs in cases with early compressive lesions of the optic tract, especially in the chiasmal or retrochiasmal regions. They reported that the VEP recordings were a sensitive and objective method for examining patients with visual field loss using full- or hemi-field stimulation or single or multichannel recordings. Flanagan and associates<sup>40</sup> reported that VEPs recorded with multichannel electrodes were useful and even more sensitive for detecting compressive lesions than subjective perimetry. In contrast, Maitland and associates<sup>1</sup> concluded that it was possible to lateralize the brain lesion, but not to predict the site of the lesion within the hemisphere. They also stated that VEP analysis is of only limited value in assessing patients with homonymous or bitemporal hemianopias.

On the basis of these findings, advanced mfVEP techniques with the dartboard pattern stimuli and recordings using bipolar occipital cross electrodes, as used in this study, enhanced the sensitivity of the VEPs in detecting postchiasmal optic nerve damage. Our findings clearly illustrate that the responses that were summed within each of the four quadrants were well-correlated with subjective perimetry in some patients. Moreover, this method was sensitive enough to detect visual field impairments even with macular sparing (Cases 7 and 10). Bradnam and associates<sup>5</sup> reported that a 90-minute check size used in their study, which is optimal for peripheral areas of the visual field, was minimally affected by central sparing of their VEP recordings. Although we are not certain whether full-field VEPs and mfVEPs are measuring the same thing, the dartboard pattern stimulus used in our study should stimulate the receptive fields optimally at each retinal eccentricity.<sup>23</sup> Therefore, they could improve the detection of incomplete hemi-field and quadrantic visual field defects and would be minimally affected by macular sparing. Further application of this technique on the large number of patients with visual field defects in the central area will be helpful in establishing whether this objective visual field testing can be used in patients with or without macular sparing.

In conclusion, there are some cases with lesions in the visual centers whose mfVEPs are not concordant with the subjective visual field. Two patients with this discordance had their hemianopsia recovered completely and three did not. We suggest that the mfVEPs originated from the primary area (area 17/V1). If the visual function arose from damage by a lesion in the higher visual centers, it is possible for the subjectively determined visual field to be dissociated from the mfVEPs. This means that damage of the visual pathway from the retina to the primary visual

cortex (area 17/V1) would decrease the mfVEPs, but the damage of the higher visual cortex could lead to a discordance between the subjective visual field test and the mfVEPs. We suggest that the primary visual cortex was not affected severely in cases 7 and 10, and the transient tissue edema or circulation disturbance after neurosurgery was responsible for the subjectively determined visual field defects. In cases 6, 8, and 9, the brain tumor was not located in the primary visual cortex, and the mfVEPs could be recorded (V1). The mfVEPs even with conventional visual field defect can be interpreted to show that the primary visual cortex is not affected. In these cases, the visual field defect that is detected by conventional subjective visual field testing may recover. However, the recovery of visual field in the two cases may be associated with the cause of the visual field defect such as edema. Further investigation will be necessary to elucidate the mechanism of the recovery.<sup>31</sup>

---

THE AUTHORS INDICATE NO FINANCIAL SUPPORT OR FINANCIAL conflict of interest. Involved in design and conduct of study (K.S., H.O.); involved in collection, management, analysis, and interpretation of the data (K.W., K.S., I.K., Y.M., Y.O., H.O.); and involved in preparation, review, and approval of the manuscript (K.W., K.S., I.K., Y.M., Y.O., H.O.).

---

## REFERENCES

1. Maitland CG, Aminoff MJ, Kennard C, Hoyt WF. Evoked potentials in the evaluation of visual field defects due to chiasmal or retrochiasmal lesions. *Neurology* 1982;32:986-991.
2. Holder GE. Pattern visual evoked potential in patients with posteriorly situated space-occupying lesions. *Doc Ophthalmol* 1985;59:121-128.
3. Wildberger HG, van Lith GH, Wijngaarde R, Mak GT. Visually evoked cortical potentials in the evaluation of homonymous and bitemporal visual field defects. *Br J Ophthalmol* 1976;60:273-278.
4. Halliday AM, Halliday E, Kriss A, et al. The pattern-evoked potential in compression of the anterior visual pathways. *Brain* 1976;99:357-374.
5. Bradnam MS, Montgomery DM, Evans AL, et al. Objective detection of hemifield and quadrantic field defects by visual evoked cortical potentials. *Br J Ophthalmol* 1996;80:297-303.
6. Oguchi Y, Toyoda M. Vector analysis of pattern VEP. *Doc Ophthalmol Proc Series* 1981;27:239-245.
7. Kardon RH, Kirkali PA, Thompson HS. Automated pupil perimetry. Pupil field mapping in patients and normal subjects. *Ophthalmology* 1991;98:485-496.
8. Lehmann D, Skrandies W. Multichannel evoked potential fields show different properties of human upper and lower hemiretina systems. *Exp Brain Res* 1979;35:151-159.
9. Kiyosawa M, Mizuno K, Hatazawa J, et al. Metabolic imaging in hemianopsia using positron emission tomography with 18F-deoxyfluoroglucose. *Am J Ophthalmol* 1986;101:310-319.



10. Palmowski AM, Sutter EE, Bearse MA Jr, et al. Mapping of retinal function in diabetic retinopathy using the multifocal electroretinogram. *Invest Ophthalmol Vis Sci* 1997;38:2586-2596.
11. Bearse MA Jr, Sutter EE. Imaging localized retinal dysfunction with the multifocal electroretinogram. *J Opt Soc Am A Opt Image Sci Vis* 1996;13:634-640.
12. Kondo M, Miyake Y, Horiguchi M, et al. Clinical evaluation of multifocal electroretinogram. *Invest Ophthalmol Vis Sci* 1995;36:2146-2150.
13. Kretschmann U, Ruther K, Usui T, Zrenner E. ERG campimetry using a multi-input stimulation technique for mapping of retinal function in the central visual field. *Ophthalmic Res* 1996;28:303-311.
14. Baseler HA, Sutter EE, Klein SA, Carney T. The topography of visual evoked response properties across the visual field. *Electroencephalogr Clin Neurophysiol* 1994;90:65-81.
15. Klistorner AI, Graham SL, Grigg JR, Billson FA. Multifocal topographic visual evoked potential: improving objective detection of local visual field defects. *Invest Ophthalmol Vis Sci* 1998;39:937-950.
16. Betsuin Y, Mashima Y, Ohde H, et al. Clinical application of the multifocal VEPs. *Curr Eye Res* 2001;22:54-63.
17. Klistorner AI, Graham SL, Grigg J, Balachandran C. Objective perimetry using the multifocal visual evoked potential in central visual pathway lesions. *Br J Ophthalmol* 2005;89:739-44.
18. Seiple W, Holopigian K, Clemens C, et al. The multifocal visual evoked potential: an objective measure of visual fields? *Vision Res* 2005;45:1155-1163.
19. Graham SL, Klistorner AI, Goldberg I. Clinical application of objective perimetry using multifocal visual evoked potentials in glaucoma practice. *Arch Ophthalmol* 2005;123:729-739.
20. Miki A, Nakajima T, Fujita M, et al. Functional magnetic resonance imaging in homonymous hemianopsia. *Am J Ophthalmol* 1996;121:258-66.
21. Slotnick SD, Moo LR. Retinotopic mapping reveals extrastriate cortical basis of homonymous quadrantanopia. *Neuroreport* 2003;14:1209-1213.
22. Horton JC, Hoyt WF. The representation of the visual field in human striate cortex. A revision of the classic Holmes map. *Arch Ophthalmol* 1991;109:816-824.
23. Goldberg I, Graham SL, Klistorner AI. Multifocal objective perimetry in the detection of glaucomatous field loss. *Am J Ophthalmol* 2002;133:29-39.
24. Hood DC, Thienprasiddhi P, Greenstein VC, et al. Detecting early to mild glaucomatous damage: a comparison of the multifocal VEP and automated perimetry. *Invest Ophthalmol Vis Sci* 2004;45:492-498.
25. Klistorner AI, Graham SL. Multifocal pattern VEP perimetry: analysis of sectoral waveforms. *Doc Ophthalmol* 1999;98:183-196.
26. Baseler HA, Sutter EE. M and P components of the VEP and their visual field distribution. *Vision Res* 1997;37:675-690.
27. Cowey A, Rolls ET. Human cortical magnification factor and its relation to visual acuity. *Exp Brain Res* 1974;21:447-454.
28. Fox PT, Miezin FM, Allman JM, et al. Retinotopic organization of human visual cortex mapped with positron-emission tomography. *J Neurosci* 1987;7:913-922.
29. Whitteridge D, Daniel PM. *The visual system: neurophysiology and psychophysics*. Berlin, Germany: Springer-Verlag; 1996:222-228.
30. Oguchi Y. Visual information processing and the mechanism of vision. Clinical application. *Nippon Ganka Gakkai Zasshi* 1998;102:850-875.
31. Graham SL, Klistorner A. *Electrophysiology: a review of signal origins and applications to investigating glaucoma*. *Aust N Z J Ophthalmol* 1998;26:71-85.
32. Jeffreys DA, Axford JG. Source locations of pattern-specific components of human visual evoked potentials. I. Component of striate cortical origin. *Exp Brain Res* 1972;16:1-21.
33. Onofrij M, Fulgente T, Thomas A, et al. Source model and scalp topography of pattern reversal visual evoked potentials to altitudinal stimuli suggest that infoldings of calcarine fissure are not part of VEP generators. *Brain Topogr* 1995;7:217-231.
34. Seki K, Nakasato N, Fujita S, et al. Neuromagnetic evidence that the P100 component of the pattern reversal visual evoked response originates in the bottom of the calcarine fissure. *Electroencephalogr Clin Neurophysiol* 1996;100:436-442.
35. Slotnick SD, Klein SA, Carney T, et al. Using multi-stimulus VEP source localization to obtain a retinotopic map of human primary visual cortex. *Clin Neurophysiol* 1999;110:1793-1800.
36. Hood DC, Greenstein VC. Multifocal VEP and ganglion cell damage: applications and limitations for the study of glaucoma. *Prog Ret Eye Res* 2001;22:201-251.
37. Fortune B, Hood DC. Conventional pattern-reversal VEPs are not equivalent to summed multifocal VEPs. *Invest Ophthalmol Vis Sci* 2003;44:1364-1375.
38. Zhang X, Hood DC. A principal component analysis of multifocal pattern reversal VEP. *J Vision* 2004;4:32-43.
39. Onofrij M, Bodis-Wollner I, Mylin L. Visual evoked potential diagnosis of field defects in patients with chiasmatic and retrochiasmatic lesions. *J Neurol Neurosurg Psychiatry* 1982;45:294-302.
40. Flanagan JG, Harding GF. Multi-channel visual evoked potentials in early compressive lesions of the chiasm. *Doc Ophthalmol* 1988;69:271-281.
41. Mashima Y, Oguchi Y. Visual evoked potential in the management of pituitary tumor during pregnancy. *Doc Ophthalmol* 1987;65:57-64.
42. Blumhardt LD, Barrett G, Halliday AM. The asymmetrical visual evoked potential to pattern reversal in one-half field and its significance for the analysis of visual field defects. *Br J Ophthalmol* 1977;61:454-461.
43. Holder GE. The effects of chiasmatic compression on the pattern visual evoked potential. *Electroencephalogr Clin Neurophysiol* 1978;45:278-280.